Electronic Properties of Nitrogene/$MoSe_2$ Heterobilayers

Rui Li*

College of Physics and Electronic Information, Luoyang Normal University, Luoyang, 471022, People's Republic of China

Received: 13.10.2020 & Accepted: 30.08.2021

Doi: 10.12693/APhysPolA.140.204 *e-mail: rli_lynu@163.com

Stacking two-dimensional crystals into van der Waals heterojunctions has recently generated enormous interest because of their novel applications in high-performance photovoltaic nanomaterials. In this paper, the electronic properties of a heterobilayer constructed with nitrogene on $MoSe_2$, denoted as nitrogene/$MoSe_2$ HBL, are studied based on the first-principles calculation. It is found that the electronic band spectrum of the nitrogene/$MoSe_2$ HBL is simply the combination of pristine nitrogene and $MoSe_2$ monolayer owing to the weak van der Waals interaction. As the vertical distance decreases, the charge redistribution in the interlayer space of the heterojunctions induces a transformation from the indirect electronic band gap of the nitrogene/$MoSe_2$ HBL towards a direct band gap. The study of the two-dimensional ultrathin nitrogene/$MoSe_2$ HBL is expected to show its potential in designing and fabricating a new generation of optoelectronic devices.

topics: electronic properties, heterobilayer, van der Waals interaction, vertical distance

1. Introduction

The successful exfoliation of graphene just over a decade ago has fostered the development of two-dimensional (2D) nanomaterials. Kinds of 2D nanomaterials, such as silicene [1–4], germanene [5–7], stanene [8–10], transition-metal dichalcogenides (TMDCs) [11–15], have been proposed theoretically and experimentally as well. It is well known that the strong chemical bonds in molybdenum dichalcogenides make them rather stable with single-layer nanostructures, thus any research related has attracted enormous attention in the scientific field. The chalcogenide derivatives of molybdenum, including MoS_2 and $MoSe_2$, belong to the large family of layered TMDCS, which are pointed to possess intriguing electronic, optical, mechanical and chemical properties [16, 17]. In addition, the analogous 2D structure of phosphorene, known as nitrogene, is predicted to be stable with low-buckle honeycomb structure [18, 19]. The semiconductor properties of it can be modulated by biaxial tensile strain, perpendicular electric field, and monolayer stacking [19].

Heterostructures, composed of layered nanomaterials, including semimetals, insulators, semiconductors, ferromagnetic nanomaterials, superconductors, and topological insulators, have been experimentally fabricated and investigated [20–30]. The materials, referred to as van der Waals (vdW) heterostructures, reveal unusual properties and new phenomena. For example, hybrid phosphorene/graphene heterobilayers possess tunable electronic and optical properties under external electric field [20, 21], therefore they can be used to fabricate high-speed devices. Moreover, varying the interfacial separation can effectively modulate the doping carrier concentration in hybrid heterobilayers after which the interlayer interactions are changed as well. It is reported that the band-gap and quasiparticle effective mass in a graphene/h-BN (hexagonal BN) bilayer can be effectively regulated by the in-plane homogeneous biaxial strain [22–25]. Those hybrid bilayers composed of transition-metal dichalcogenides monolayers and MXene belong to the type-II band offset [26–29] in which the conduction band minimum and valence band maximum come from different 2D materials [30]. Therefore, the investigation of a heterobilayer system is highly important for further research and possible application of 2D nanomaterials.

The excellent properties of TMDCs make them a potential substrate to support other 2D monolayers. Here, we are interested in the electronic properties of the nitrogene/$MoSe_2$ heterobilayer and the influence of varying the vertical distance on it. In our paper, the electronic properties of the heterobilayer constructed with nitrogene on $MoSe_2$ are studied based on the first-principle calculation. It is found that the electronic band spectrum of the nitrogene/$MoSe_2$ HBL are simply a combination of pristine nitrogene and $MoSe_2$ monolayer owing

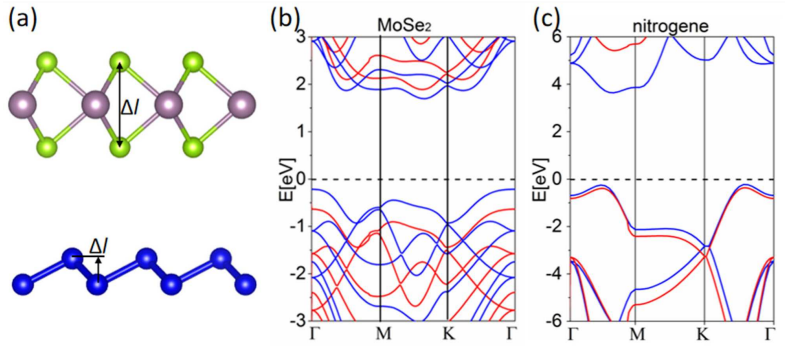

Fig. 1. The side views of $MoSe_2$ and nitrogene monolayer, in which the buckle height Δl is indicated (a). The purple, green, and blue balls denote, respectively, Mo, Se, and N atoms. The electronic band spectrum of the $MoSe_2$ (b), and the nitrogene monolayer (c), respectively, were calculated with the GGA (blue lines) and the hybrid functional HSE06 (red lines). The black dashed lines indicate the Fermi level, which has been set to zero.

to the weak vdW interaction. As the vertical distance of the heterobilayer is decreasing, the nitrogene/$MoSe_2$ HBL realizes a transformation from the indirect electronic band-gap semiconductor to the direct electronic band-gap semiconductor.

The next part of this paper is organized as follows: In Sect. 2, the computational details of the geometrical structures and the electronic band spectrum of $MoSe_2$ and the nitrogene monolayer are described. In Sect. 3, numerical results and the related discussion are given while the conclusions are provided in Sect. 4.

2. Computational method and model

All the calculations were performed based on density functional theory (DFT) as implemented in the Vienna *ab initio* simulation package (VASP) [31, 32]. The exchange-correlation function is treated within the generalized gradient approximation (GGA) and parametrized by the Perdew–Burke–Ernzerhof (PBE) formula [33]. Moreover, the electron–ion potential is described by the projected augmented wave (PAW) potential [34, 35] and a kinetic energy cutoff of 500 eV is selected for the plane wave expansion. Integrations over the first Brillouin zone are performed using the $15 \times 15 \times 1$ Monkhorst–Pack k-point grid, and $35k$-points in each high symmetry line are used to calculate the electronic bands of the hybrid nitrogene/$MoSe_2$ HBL. The valence electron configurations considered are Mo ($4p5s4d$), Se ($4s4p$) and N ($2s2p$), respectively. Both the lattice vectors and atomic positions are fully relaxed by minimizing the quantum mechanical stresses and forces. The convergence for energy is chosen as 10^{-5} eV between two steps and the structural optimization is obtained until the Hellmann–Feynman forces acting on each atom are less than 0.01 eV/Å. In addition, the non-bonding van der Waals interaction is incorporated by adding a semi-empirical dispersion potential to the conventional Kohn–Sham DFT energy, through a pairwise force field following Grimme's DFT-D_2 method [36]. Moreover, a dipole correction is adopted to cancel the errors of electrostatic potential, atomic forces, and total energy.

TABLE I

The lattice constants (a), bond lengths, buckle height (Δl) and band gaps (E_g) of $MoSe_2$ and nitrogene monolayer.

	a [Å]	Bond length [Å]	Δl [Å]	E_g [eV]	
				GGA	HSE06
nitrogene	2.29	1.50	0.70	3.89	5.78
$MoSe_2$	3.32	2.54	3.34	2.08	2.52

The geometrical structures of $MoSe_2$ and a buckle nitrogene monolayer are firstly optimized in a primitive cell to determine the stable structures. The calculated parameters of $MoSe_2$ and the buckle nitrogene monolayers, including the lattice constants (a), the bond lengths, the buckle height (Δl) and the band gaps (E_g), are shown in Table I. As shown in Fig. 1a, the buckle height Δl of $MoSe_2$ is defined as the vertical distance of the upper and lower Se atoms in $MoSe_2$, and that of nitrogene indicates the vertical distance of N atoms in nitrogene. These results agree well with the theoretical investigations [18, 19, 37]. The electronic band spectra, calculated with the GGA and the hybrid density function HSE06 (with the same screening parameters of PBE and HF exchange), are given in Fig. 1. The band gaps of $MoSe_2$ and the nitrogene monolayer are, respectively, 2.08 eV and 3.89 eV for the GGA calculation. In turn, the band gaps for the HSE06 calculation are increased to 2.52 eV and 5.78 eV. As shown in Fig. 1, it is found that the hybrid density function HSE06 does not influence the spectrum trend, but only the band gaps of the monolayers are enlarged. Therefore, our numerical results are based on the GGA.

3. Numerical results and discussion

To construct the nitrogene/$MoSe_2$ HBLs, a commensurable supercell with 2×2 lateral periodicity of $MoSe_2$ and 3×3 lateral periodicity of nitrogene in the x–y plane is employed (see Fig. 2a). The lattice mismatches between the supercell of nitrogene and $MoSe_2$ are about 3.6%, in contrast to nitrogene, i.e., these mismatches are reasonably small in comparison with the other reported heterostructures [20–25]. Additionally, to avoid the spurious interaction between the periodic images, the vacuum region along the direction normal to the 2D plane is set to 25 Å. The vertical distance (Δh) between nitrogene and $MoSe_2$ is defined as the vertical distance between the lower N atoms in the nitrogene layer and the upper Se atoms in $MoSe_2$, as shown in the side view in Fig. 2b.

To determine the most stable geometrical structure of the nitrogene/$MoSe_2$ HBL, the artificial constructions of it are fully optimized from different initial structures, which are obtained by adjusting the relative position of nitrogene and $MoSe_2$ layers in the x–y plane. It is found that those different initial structures converge to the same geometrical structure during the geometrical optimization, in which $\Delta h = 3.43$ Å. The optimized lattice parameters of the nitrogene/$MoSe_2$ HBL are 6.80 Å, which is about 0.18 Å larger than the 2×2 $MoSe_2$ layer, and 0.08 Å smaller than the 3×3 nitrogene layer.

Our further calculations show that the influence of the little variation of the unit cell on pristine $MoSe_2$ and nitrogene is ignorable. In the HBL, the buckle height Δl of nitrogene is 0.70 Å, which is the same as in the case of the free-standing one.

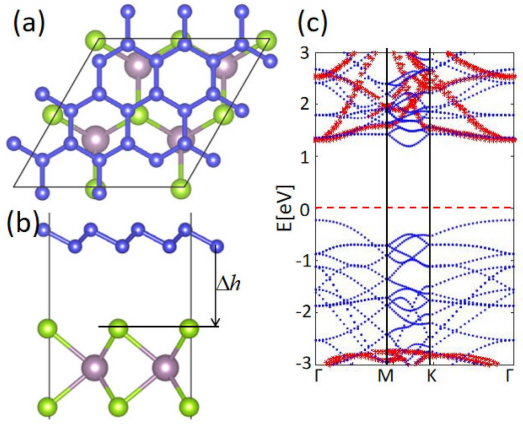

Fig. 2. The top view (a) and the side view (b) of the nitrogene/$MoSe_2$ HBLs, in which the optimum hybrid cells are denoted by rhombuses. The purple, green, and blue balls depict, respectively, Mo, Se, and N atoms. In the electronic band spectrum of the nitrogene/$MoSe_2$ HBL (c), the blue dots come mainly from the $MoSe_2$ layer, and the red dots are mainly contributed by the nitrogene layer. The red dashed line indicates the Fermi level, which has been set to zero.

Firstly, the formation energy is calculated to evaluate the stability of the nitrogene/$MoSe_2$ HBL. We use the relation

$$E_f = E_{\text{total}} - E_{\text{MoSe}_2} - E_N, \tag{1}$$

where E_{total}, E_{MoSe_2}, and E_N are the total energies, respectively, of the hybrid nitrogene/$MoSe_2$ HBL, pristine $MoSe_2$, and the buckle nitrogene monolayer. A negative E_f refers to a stable adsorption structure. The calculated formation energy of the nitrogene/$MoSe_2$ HBL is about -3.93 eV per supercell, which implies a stable hybrid heterostructure with van der Waals interaction.

Now, the result of calculation of the electronic band spectrum of nitrogene/$MoSe_2$ is shown in Fig. 2c. In the band structure, the blue circles come mainly from the $MoSe_2$ layer and the red stars are mainly contributed by the nitrogene layer. Owing to the weak van der Waals interaction, the hybridization between nitrogene and $MoSe_2$ monolayer is small. Thus, the electronic band of the nitrogene/$MoSe_2$ HBL is simply the combination of the electronic bands of $MoSe_2$ and those of the nitrogene monolayer. From the electronic band spectrum, it is seen that the valence band of the hybrid HBL is mastered both by $MoSe_2$ and nitrogene layers, while the conduction band is dominated by the $MoSe_2$ layer. Comparing with the isolated $MoSe_2$ and nitrogene monolayer, the conduction bands of $MoSe_2$ and nitrogene come closer to the Fermi level, respectively, at 1.06 eV and 1.13 eV. The conduction bands formed by nitrogene occur below the Fermi level at about -2.75 eV. In the nitrogene/$MoSe_2$ HBL, the band gap of the $MoSe_2$ layer is 1.42 eV, which is 0.66 eV smaller than the pristine $MoSe_2$ monolayer. In turn, the band gap of nitrogene layer is 4.07 eV, which is about 0.18 eV larger than the nitrogene monolayer. As a result, the band gap of the nitrogene/$MoSe_2$ HBL is 1.42 eV, which is dominated by the conduction and valence bands of the $MoSe_2$ layer.

To investigate the influence of spacing between nitrogene and $MoSe_2$ layers on the electronic properties of the nitrogene/$MoSe_2$ HBL, their electronic bands with different Δh are calculated. The corresponding results are provided in Fig. 3a–e, in which the red stars are mainly induced by the nitrogene layer and the blue dots come mainly from the $MoSe_2$ layer. It is found from the band structures in Fig. 3 that the vertical distance decreases, the integrity of the conduction band lines of the system comes closer to the Fermi level but the system's valence bands change little. As a result, the band gaps of the nitrogene/$MoSe_2$ HBL become smaller as the vertical distance Δh decreases. The band gaps of the nitrogene/$MoSe_2$ HBL varying with Δh are provided in Fig. 3f.

To properly interpret the influence of the vertical distance on the electronic behavior, the total density of states (tDOSs) of nitrogene and $MoSe_2$ layer in the nitrogene/$MoSe_2$ HBL are respectively

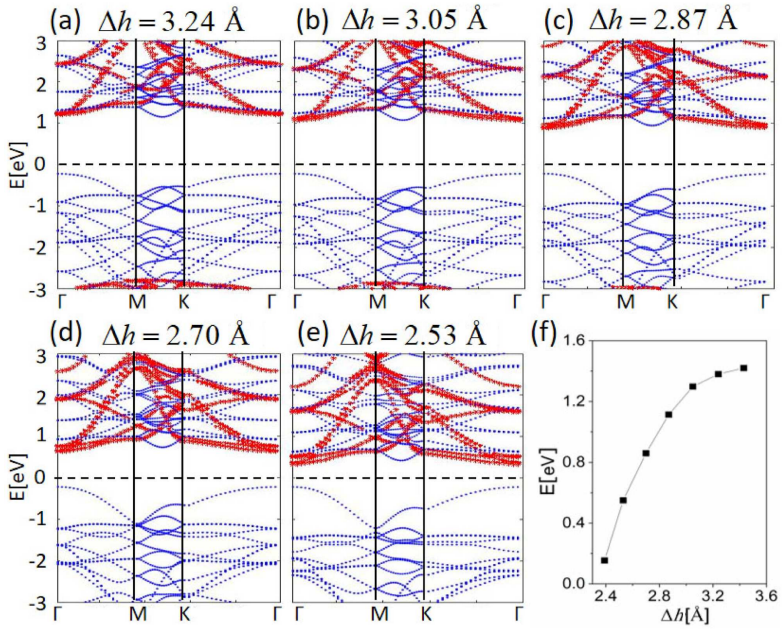

Fig. 3. The electronic band spectrum of the nitrogene/$MoSe_2$ HBL, respectively, with (a) $\Delta h = 3.24$ Å, (b) $\Delta h = 3.05$ Å, (c) $\Delta h = 2.87$ Å, (d) $\Delta h = 2.70$ Å, (e) $\Delta h = 2.53$ Å. The black dashed lines indicate the Fermi level, which has been set to zero. The blue and red dots come from $MoSe_2$ and nitrogene, respectively. The band gaps of the nitrogene/$MoSe_2$ HBL (f) vary with Δh.

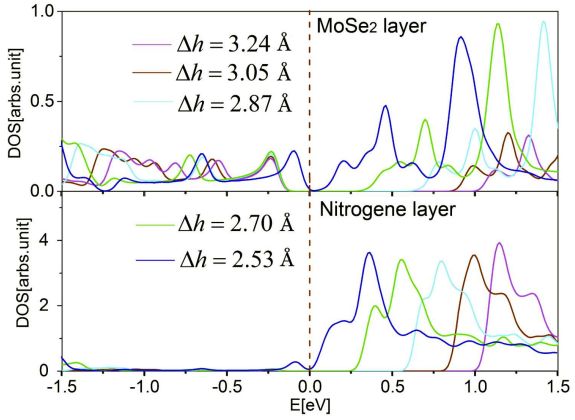

Fig. 4. The tDOSs of (a) $MoSe_2$ and (b) the nitrogene layer in the nitrogene/$MoSe_2$ HBL, respectively, with (a) $\Delta h = 3.24$, 3.05, 2.87 Å, (b) 2.70, 2.53 Å. The red dashed lines indicate the Fermi level, which has been set to zero.

given in Fig. 4a and b. As one can see, the results are consistent with the variation of the band spectrum shown in Fig. 3a–e. On the one hand, both conduction bands of nitrogene come closer to the Fermi level to result in smaller band gaps. Such a conclusion may be drawn based on the band spectrum in Fig. 3a–e and the tDOSs in Fig. 4. On the other hand, the difference between the indirect and direct band gaps is smaller as Δh is decreasing, and the hybrid system transforms into the direct band when Δh is decreasing. For example, at $\Delta h = 3.24$ Å and $\Delta h = 3.05$ Å, the indirect band gaps of the nitrogene/$MoSe_2$ HBL are, respectively, 1.54 eV and 1.44 eV, and the direct band gaps of the nitrogene/$MoSe_2$ HBL are, respectively, 1.42 eV and 1.38 eV. Note that at $\Delta h = 2.87$ eV, the nitrogene/$MoSe_2$ HBL changes into direct band gap, where the direct electronic band gap is 1.11 eV.

It is known that the Se atom and the N atom manifest different electronegativities (selenium 2.55 and nitrogen 3.04), and therefore nitrogene has a deeper potential well than selenium. As a result, theoretically, when nitrogene contacts with $MoSe_2$, electrons tend to depart from selenium to nitrogene, resulting in an n-type doping of nitrogene in the nitrogene/$MoSe_2$ HBL. Here, to understand the charge transfer mechanism between nitrogene and $MoSe_2$ in the vdW HBL, the plane-integrated electron density differences are calculated according to the following equation:

$$\Delta\rho = \rho_{\text{total}} - \rho_{MoSe_2} - \rho_{\text{N}}, \tag{2}$$

where ρ_{total}, ρ_{MoSe_2}, and ρ_{N} are the plane-averaged electron densities of the nitrogene/$MoSe_2$ HBL, the $MoSe_2$ layer, and the nitrogene layer, respectively. The electron redistribution upon the formation of the interface is depicted in Fig. 5.

It is observed that there is no charge transfer between nitrogene and $MoSe_2$ monolayer due to the weak van der Waals interaction between nitrogene and $MoSe_2$ layer. However, as the vertical distance decreases, an obvious charge redistribution is observed in the interlayer space of the heterojunctions, as shown in Fig. 5. It can be seen that the charge

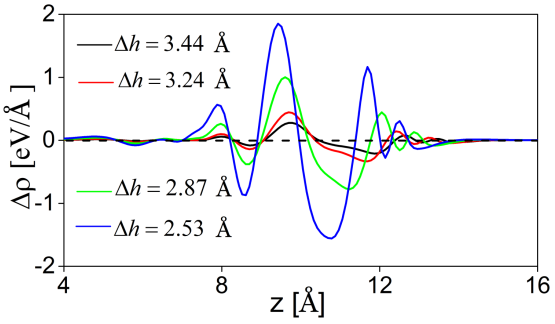

Fig. 5. Plane-integrated electron density difference of the nitrogene/$MoSe_2$ HBL along the vertical direction, with Δh = 3.44, 3.24, 2.87, and 2.53 Å, respectively.

in the nitrogene/$MoSe_2$ HBL is gradually accumulated at the topmost Se layer of $MoSe_2$ monolayers. However, it is dissipated at the second Se layer of the $MoSe_2$ layer, resulting from the increased electrostatic interaction between nitrogene and $MoSe_2$ layers.

4. Conclusion

Based on the first-principle calculation, the electronic properties of the heterobilayer constructed with nitrogene on $MoSe_2$ are investigated. A weak van der Waals interaction between nitrogene and $MoSe_2$ monolayer is assumed. It is found that the electronic band spectrum of the nitrogene/$MoSe_2$ HBL are simply the combination of pristine nitrogene and $MoSe_2$ monolayer. The conduction bands are both dominated by nitrogene and $MoSe_2$ layers while the valence bands are mastered by the $MoSe_2$ layer. As the vertical distance decreases, the conduction bands come close to the Fermi level to result in a smaller indirect band gap of the nitrogene/$MoSe_2$ HBL. As Δh is further decreasing, e.g., at Δh = 2.87 Å, the indirect band gap transforms into the direct band gap due to the charge redistribution in the interlayer space of the heterojunctions. The study of the two-dimensional ultrathin nitrogene/$MoSe_2$ HBL is expected to show its potential in designing and fabricating a new generation of optoelectronic devices.

Acknowledgments

This work was supported by the National Natural Science Foundation of China (Grant No. 11504156), the Key Scientific Research Project of Henan Provincial Universities (Grant No. 17B140004), and the Excellent Team of Spectrum Technology and Application of Henan Province (Grant No. 18024123007). We also acknowledge the support from the High Performance Computing Center of Nanjing University.

References

[1] C.-C. Liu, H. Jiang, Y. Yao, *Phys. Rev. B* **84**, 1954301 (2011).

[2] L. Chen, C.-C. Liu, B. Feng, X. He, P. Cheng, Z. Ding, S. Meng, Y. Yao, K. Wu, *Phys. Rev. Lett.* **109**, 056804 (2012).

[3] S. Cahangirov, M. Topsakal, E. Aktürk, H. Sahin, S. Ciraci, *Phys. Rev. Lett.* **102**, 2368041 (2009).

[4] C.-C. Liu, W. Feng, Y. Yao, *Phys. Rev. Lett.* **107**, 0768021 (2011).

[5] Z.Y. Ni, Q.H. Liu, K.-C. Tang, J.-X. Zheng, J. Zhou, R. Qin, Z.-X. Gao, D.-P. Yu, J. Lu, *Nano Lett.* **12**, 113 (2012)10.1021/nl203065e.

[6] C. Si, J.-W. Liu, Y. Xu, J. Wu, B.L Gu, W.H. Duan, *Phys. Rev. B* **89**, 1154291 (2014).

[7] C.-C. Liu, W.X. Feng, Y.G. Yao, *Phys. Rev. Lett.* **107**, 0768021 (2011).

[8] F.-F. Zhu, W.-J. Chen, Y. Xu, C.-L. Gao, D.-D. Guan, C.-H. Liu, D. Qian, S.-C. Zhang, J.-F. Jia, *Nat. Mater.* **14**, 1020 (2015).

[9] P.Z. Tang, P.C. Chen, W.D. Cao, H.Q. Huang, *Phys. Rev. B* **90**, 1214081 (2014).

[10] H.S. Zhang, T. Zhou, J.Y. Zhang, B. Zhao, Y.G. Yao, Z.Q. Yang, *Phys. Rev. B* **94**, 235409 (2016).

[11] A. Ayari, E. Cobas, O. Ogundadegbe, M.S. Fuhrer, *J. Appl. Phys.* **101**, 014507 (2007).

[12] A. Ramasubramaniam, D. Naveh, E. Towe, *Phys. Rev. B* **84**, 205325 (2011).

[13] J. Kim, S. Byun, A.J. Smith, J. Yu, J.X. Huang, *J. Phys. Chem. Lett.* **4**, 1227 (2013).

[14] Y. Song, H. Dery, *Phys. Rev. Lett.* **111**, 026601 (2013).

[15] F.A. Rasmussen, K.S. Thygesen, *J. Phys. Chem. C* **119**, 13169 (2015).

[16] S.W. Luo, X. Qi, L. Ren et al., *J. Appl. Phys.* **116**, 164304 (2014).

[17] H.D. Abruna, G.A. Hope, A.J. Bard, *J. Electrochem. Soc.* **129**, 2224 (1982).

[18] Y. Kadioglu, O. Üzengi Aktürk, S. Ciraci, *J. Phys. Chem. C* **121**, 6329 (2017).

[19] J.-S. Li, W.-L. Wang, D.-X. Yao, *Sci. Rep.* **6**, 34177 (2016).

[20] W. Hu, T. Wang, J.-L. Yang, *J. Mater. Chem. C* **3**, 4756 (2015).

[21] X.-Q. Tian, L. Liu, Y. Du, J. Gu, J.-B Xu, B.I. Yakobson, *Phys. Chem. Chem. Phys.* **17**, 1831 (2015).

[22] W. Gannett, W. Regan, K. Watanabe, T. Taniguchi, M. Crommie, A. Zettl, *Appl. Phys. Lett.* **98**, 2421051 (2011).

[23] Z. Liu, L. Song, S. Zhao, J. Huang, L. Ma, J. Zhang, J. Lou, P.M. Ajayan, *Nano Lett.* **11**, 2032 (2011).

[24] J. Sławinska, I. Zasada, Z. Klusek, *Phys. Rev. B* **81**, 1554331 (2010).

[25] Y.-L. Mao, Z.-Q. Xie, J.-M. Yuan, S.-H. Li, Z. Wei, J.-X. Zhong, *Physica E* **49**, 111 (2013).

[26] K.F. Mak, C. Lee, J. Hone, J. Shan, T.F. Heinz, *Phys. Rev. Lett.* **105**, 1368051 (2010).

[27] S. Tongay, J. Zhou, C. Ataca, K. Lo, T.S. Matthews, J. Li, J.C. Grossman, J. Wu, *Nano Lett.* **12**, 5576 (2012).

[28] B. Radisavljevic, A. Radenovic, J. Brivio, V. Giacometti, A. Kis, *Nat. Nanotechnol.* **6**, 147 (2011).

[29] H. Sahin, S. Tongay, S. Horzum, W. Fan, J. Zhou, J. Li, J. Wu, F.M. Peeters, *Phys. Rev. B* **87**, 1654091 (2013).

[30] Z. Ma, Z. Hu, X. Zhao, Q. Tang, D. Wu, Z. Zhou, L. Zhang, *J. Phys. Chem. C* **118**, 5593 (2014).

[31] G. Kresse, J. Furthmüller, *Comput. Mater. Sci.* **6**, 15 (1996).

[32] G. Kresse, J. Hafner, *Phys. Rev. B* **47**, 558 (1993).

[33] J.P. Perdew, K. Burke, M. Ernzerhof, *Phys. Rev. Lett.* **77**, 3865 (1996).

[34] P.E. Blöchl, *Phys. Rev. B* **50**, 17953 (1994).

[35] G. Kresse, D. Joubert, *Phys. Rev. B* **59**, 1758 (1999).

[36] S. Grimme, *J. Comput. Chem.* **27**, 1787 (2006).

[37] Y.D. Ma, Y. Dai, M. Guo, C.W. Niu, J.B. Lu, B.B. Huang, *Phys. Chem. Chem. Phys.* **13**, 15546 (2011).